Recognition of Volcanoes on Venus using Correlation Methods

Charles R. Wiles[1,2]

M.R.B. Forshaw[1]

[1]Image Processing Group, [2]Planetary Science Group
Department of Physics and Astronomy, University College London
London WC1E 6BT, UK

Abstract

Radar images of 95% of the surface of Venus have been obtained by the *Magellan* spacecraft at resolutions of 100-300 m. The surface area covered is 3 times the total land-mass area of the Earth; this corresponds to a data volume of about 10^{11} bytes.

A large population of volcanoes has been observed in this data set. Measurements of these features are essential for a full understanding of Venusian geology. The scale of the task, however, precludes the use of manual methods to make these measurements. An algorithm for the automated location and counting of these volcanoes is therefore being developed.

The noisy nature of the data makes it appropriate to use correlation-based techniques to recognise the features. A least-squares-error template matching algorithm has been implemented, which includes local DC removal and contrast normalisation.

Preliminary experimental results from running the algorithm on Magellan data are presented, along with the corresponding measurements of expert human observers. Because there is no ground truth information for Venus, it has also been necessary to undertake a control experiment, using simulated radar images of artificial terrain. The results of this experiment are also included and compared with theoretical predictions: their implications for the calibration of both human and automated measurements are discussed.

1 Introduction

The main objective of the Magellan mission is to increase knowledge about the geological history and geophysics of the planet Venus, by mapping its surface [1]. To accomplish this, a spacecraft containing a synthetic aperture radar (SAR) instrument was inserted into orbit about Venus in August 1990. Since then, the spacecraft has returned SAR images of 95% of the planet's surface at resolutions of between 100 and 300 m. Because Venus does not possess any oceans, the surface area mapped by Magellan is over three times the total area of all the land masses on Earth; this represents an image data volume of almost 100 Gb [2].

The fact that its bulk properties are so similar to Earth's makes Venus a unique and important planetary comparison. By studying its geology and surface processes it is hoped that our understanding of the formation and evolution of the Earth will be

BMVC 1992 doi:10.5244/C.6.30

improved. Unfortunately, it is impossible to observe Venus' surface using conventional remote sensing techniques because it is continuously obscured by optically opaque clouds. However, Magellan's radar, operating at a wavelength of 12.6 cm, is able to penetrate the cloud cover.

Both the Magellan and earlier (low-resolution) Venera 15/16 SAR data have revealed that small volcanoes are a prevalent feature on the Venusian surface. These edifices, which are predominantly low shield volcanoes <15 km in diameter, have been extensively described by several earlier workers (eg. [3,4]). Their abundance indicates that volcanism has been of fundamental importance to Venus' evolution. The fact that they are also extremely widespread makes the volcanoes an important statistical tool for studying Venus' geological history. Measuring their global population, spatial distribution and size-frequency distribution would provide important information about both the geological and geophysical processes on Venus.

However, from previous work it is estimated that the global population of small volcanic features on Venus is of the order of 5×10^6 [3]. This, together with the vast size of the Magellan data set (described above), means that even a preliminary visual survey would take a trained observer at least 5 years. To make detailed, global measurements would therefore be extremely time-consuming and prone to error. It is thus desirable that an automated method be developed for the consistent identification and measurement of these features.

This paper discusses one such method which is based on correlation techniques, specifically a template matching algorithm. There is an additional problem associated with this task, however: the total lack of ground truth information against which to calibrate the algorithm. Consequently, the paper also describes a control experiment which involved generating artificial SAR images of synthetic terrain, designed to emulate closely real Magellan imagery of the small volcanoes.

2 Magellan data characteristics

Magellan's SAR transmits pulses of coherent, microwave radiation perpendicular to its flight-path and records the back-scattered echoes. These echoes are then processed to form images by analysing their intensity, time-delay and frequency-shift. Multiple sampling allows the spatial resolution of a larger antenna to be synthesised.

This image formation mechanism is fundamentally different to the way in which images at visible wavelengths are produced. Consequently, SAR images possess certain properties which set them apart from conventional images. The slant-range/doppler SAR coordinate system is very different from the coordinate system of a traditional image and leads to different types of geometric distortions. The much longer wavelengths involved mean that radar reflectance characteristics are also different: radar back-scatter strength is governed by the topography, roughness and electrical properties of a surface in a complex and incompletely understood manner. Finally, since they are produced from coherent illumination, SAR data inherently suffer from the effects of speckle noise, giving them a grainy texture.

These characteristics can place additional demands on pattern recognition algorithms used to analyse SAR data. For example, both the degree of geometric distortion and the dominant back-scatter mechanism observed, depend strongly on the radar incidence angle, which may not remain constant (as is the case with Magellan).

Due to technical constraints, Magellan's polar orbit is highly elliptical, which causes significant variation in the SAR imaging parameters. The range resolution varies from 110 to 280 m, the nominal incidence angle changes from 17° to 47° and

the number of looks (which affects the speckle noise) goes from 5 to 17. Thus, in the Magellan data, similar features can appear quite different, depending on which combination of parameters were in force at that stage of the mapping sequence.

Every orbit, the spacecraft maps a swath that is 16000 km long and 25 km wide. The SAR data undergo several stages of processing to convert them into grey-level images. This processing includes both geometric and radiometric corrections, followed by resampling to give a uniform pixel spacing of 75 m. Finally, the image swaths are mosaicked together into data products known as *MIDR*s. Each MIDR contains 56 Mb of data, in the form of an 8192x7168 array of 8-bit pixels. To cover the entire planet, 1650 such MIDRs are required. (A full description of the Magellan mission is given in [5]).

3 Description of algorithm

Because the SAR images are inherently noisy, it is not possible to employ feature-detection methods which are based on edges or contours. Instead area-based methods must be used, foremost amongst which is the classical correlation of a template with the scene. In practice, classical correlation is unsatisfactory because it breaks down when faced with variations in background brightness or structures whose contrast differs from that of the template.

The correlation process must be carried out in spatial coordinates to allow for the locally-varying DC removal and contrast normalisation. These corrections are essential if low-contrast features are to be detected. Although correlation could be carried out using global FFT techniques it would be extremely inefficient to implement such local corrections using these methods.

The algorithm which is used for this work is known to be statistically robust and relatively insensitive to noise [6]. For a given position within an image *(p,q)*, using a template of size N x N, the correlation function $C(p,q)$ is defined as follows

$$\mathbf{C(p,q)} = \sum_{i,j=0}^{N-1} \left[\left[\frac{(t(i,j) - \bar{t})}{\left[\sum_{k,l=0}^{N-1} (t(k,l) - \bar{t})^2 \right]^{0.5}} \right] - \left[\frac{(I(i+p,j+q) - \bar{I})}{\left[\sum_{m,n=0}^{N-1} (I(m+p,n+q) - \bar{I})^2 \right]^{0.5}} \right] \right]^2 \quad (1)$$

where: t and I represent the pixel values of the template and the image respectively; and $\bar{t}$ and $\bar{I}$ are the mean template value and the local mean image value. The t and $\bar{t}$ values are independent of p and q, and are calculated prior to correlation. Here, *(p,q)* defines the top-left corner of the portion of the image covered by the template. This would produce an offset in the final detected position, so, in practice, a correction is applied to centre the coordinates recorded by the algorithm.

The features being searched for, small shield volcanoes, exhibit a wide range of morphological types (see fig. 1). For each volcanic type, a distinct set of templates would have to be employed, to ensure successful matching. This is in addition to the usual requirement of using a range of template sizes to permit recognition of features at differing scales. Together with the variable imaging geometry already described, these considerations make the problem of automatically recognising all of the volcanoes in the Magellan data set very demanding.

Template-matching is a numerically intensive process. For correlations undertaken in the spatial domain, the number of calculations required for a template of size N, in a scene of size M, is proportional to N^2M^2. The small volcanoes are typically 3-4 km in diameter, or 40-50 pixels in the Magellan images. However, it is estimated

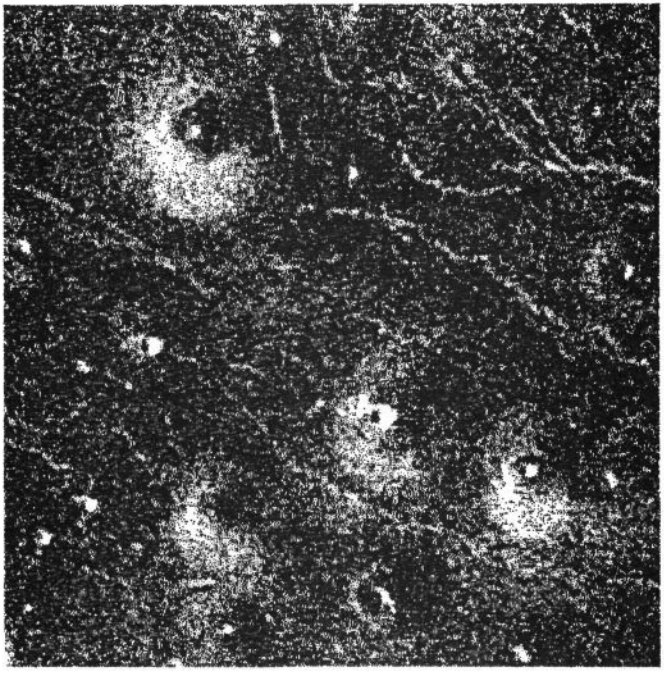

Fig. 1 Example of a Magellan SAR image showing various types of small volcanoes: many possess summit pits.

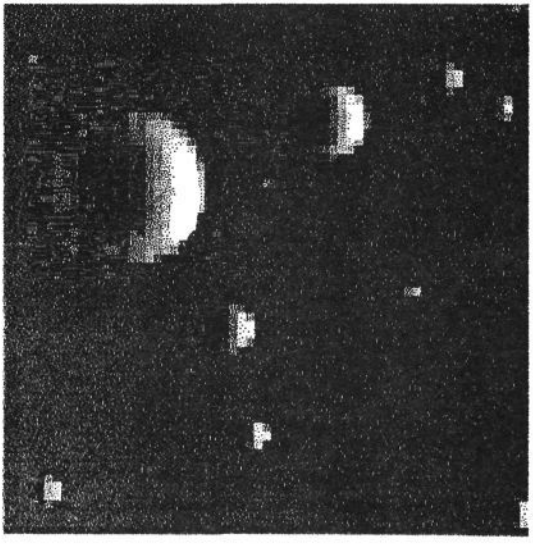

Fig. 2 Radar image simulation of artificial pits of several sizes, prior to addition of speckle noise. Note, however, inclusion of random surface texture.

that 85% of the volcanoes possess central features known as summit pits [4]. Because these pits have high visual contrast, they are discernible at sizes of about 5 pixels, though they are typically about 10 pixels across, with maximum diameters of 20 pixels or more. This means that they can be matched much more rapidly than can the (considerably larger) complete edifices (since $N_{pit}^2 \ll N_{volcano}^2$). The pits are also more regular in appearance than the volcanic edifices. For these reasons it was decided to concentrate initially on recognising the summit pits. To further reduce processing times, it was also decided that preliminary experiments should be performed using sub-scenes from MIDRs of just 512x512 pixels (ie. to restrict M^2).

4 Generation of synthetic data

There are two types of error to which all forms of feature identification are subject: failures, or 'false negatives' (ie. the number of real features missed); and false alarms, or 'false positives' (ie. the number of non-existent features identified). When dealing with real, noisy data it is unlikely that pattern recognition algorithms can ever achieve 100% success rates (ie. zero false negatives) whilst making no spurious identifications (ie. zero false positives). It is therefore highly desirable to be able to assess the absolute accuracy of any chosen algorithm.

With Magellan data, the lack of ground truth forces a dependence upon uncalibrated human observations against which to compare recognition algorithms. For this work, it was therefore decided to undertake a control experiment, in order to calibrate the ability both of humans and the machine to identify small 'pit-like' features, in the presence of speckle noise. To achieve this, it has been necessary to produce simulated radar images of synthetic terrain, designed to resemble Magellan imagery as closely as possible. This procedure involved several stages –

1. Production of artificial terrain:
The requirement was for a digital elevation model (DEM) to be produced which would closely resemble the morphology of volcanic summit pits on Venus. The characteristics of the shape required were estimated by expert interpretation of Magellan images of typical pits and by using knowledge of analogous features on Earth. A 3-D DEM was then generated using B-splines with ten free parameters, which were varied until the correct shape was obtained. The parameters controlled morphometric quantities such as pit depth and diameter. Once a satisfactory DEM was obtained, simulated surface texture was included by adding small random height perturbations. To reduce large discontinuities, the roughened surface was then smoothed using 3x3 height-averaging.

2. Radar image simulation:
There are several means by which simulated radar images of a DEM can be obtained. For this project it was decided to employ a radar image simulation (see [7]). This technique involved several phases. First, an illumination vector was defined according to the nominal radar incidence angle that was being used for the simulation. By considering the DEM to consist of surface facets, a radar reflectance map was then obtained using simple vector geometry and a suitable, standard back-scatter model. This map contained the radiometric components of the simulated image. However, it was also necessary to model the geometric properties of radar imagery. This was achieved by simulating the effects of slant-range binning. The bin sizes were made to be significantly larger than the reflectance map pixels, since in a real radar image, the back-scattered signal is considered to be produced by returns from many individual scatterers within a

resolution element.

Binning occurred in the axis of the reflectance map that was parallel to the illumination vector (the *range* direction), utilising the DEM once again to ensure correct simulation of the geometric distortions. Since the range resolution was now considerably coarser than that in the other axis, cross-range averaging was performed to make the resolutions in both axes comparable; a similar procedure is used in real SAR processing to reduce the effects of speckle. Finally, the pixel brightness values were adjusted to emulate the specific effects of the Magellan SAR processing sequence (fig. 2 shows examples of the simulated radar images of artificial pits of various sizes).

The radar image simulation was now complete, except for the effects of speckle. These were modelled separately and added to the final image (see below).

3. Scene generation:

Simulated radar images were generated for a whole range of pit diameters, from 2-16 pixels. Pre-determined numbers of these different-sized images were then added to a uniform background (possessing the mean Magellan pixel brightness) to yield scenes with a variety of pit size distributions. The distributions used included exponential, 1/radius and uniform.

The algorithm placed each pit at a random location within the 512x512 scene and stored in a table both the coordinates and the size of the pit. A check was first made, however, to ensure that the randomly generated location for the pit, was entirely within the scene and also that another pit had not been previously placed there. The second restriction was enforced to avoid small pits being covered by larger ones (fig. 3 shows one such artificial scene).

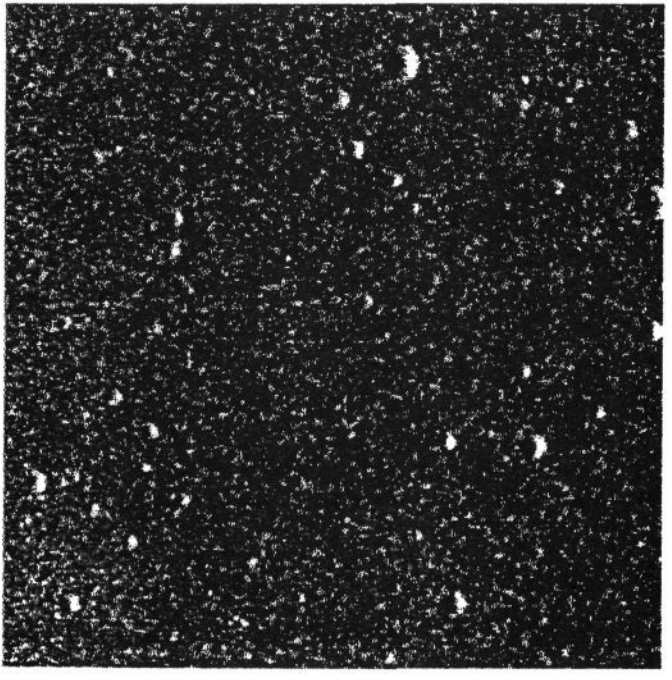

Fig. 3 Simulated radar scene containing pits of various sizes: includes speckle noise.

4. Addition of speckle:
Speckle noise is observed in any images produced by coherent radiation. With SAR images, it results from the interference of returns from many radar scatterers within a resolution element. Speckle can be reduced by making several statistically independent observations, or *looks*, of a target and averaging them. Magellan always obtains images comprising at least five looks.

SAR speckle can be modelled as a random multiplicative noise source with a Rayleigh distribution. The effects of speckle were therefore simulated by using a Rayleigh random number generator to produce a 512x512 'speckle' image, with a mean value of 1.0. To obtain 'multiple looks', several such images were generated using different random number seeds. For this experiment, five of the speckle images were averaged together. Finally, since speckle noise is multiplicative, the artificial scene was multiplied by the five-average speckle image, pixel by pixel.

5. Resolution degradation:
The last stage of the data simulation, was to emulate the resampling of Magellan images, described in section 2. To achieve this it was decided to employ 3x3 local-neighbourhood blurring. The blurring kernel was chosen so as to mimic the resampling of a typical Magellan resolution cell (150x110 m) into 75x75 m pixels.

Fig. 3 is the final product of one such scene simulation, which was used in the control experiments described in section 6.1.

5 Theoretical correlation performance

This section briefly describes a theory which has been developed to predict the performance of the correlation algorithm with the test data generated using the procedure outlined above. Consider a template of area A pixels, containing the noise-free image of a pit: assume that the pixel values in the template are gaussian-distributed with zero mean and some known standard deviation. The template is shifted across the scene and is correlated with the scene data according to expression (1). Note that both the scene data lying within the current window and the template data are first normalised to unit variance. At points in the scene where there is only a uniform background which is corrupted by speckle, then the correlation function may be written in the simplified form:

$$C = \sum_{A} (t_{norm} - B_{norm})^2 \qquad (2)$$

where t_{norm} represents the normalised template data values and B_{norm} represents the independently normalised, noisy background values. C is a sum of A independent samples, each of variance 2, since both t_{norm} and B_{norm} have unit variance. The expectation value for C , $\langle C \rangle$, is therefore $2A$ and its standard deviation, σ, is approximately $\sqrt{2A}$. By making similar approximations it can also be shown that when the template overlays a portion of the scene which contains a noisy version of the template data, the value for $\langle C \rangle$ is $\simeq A$, with a standard deviation of $\sqrt{2A}$.

A further assumption is made, that the background values are also gaussian-distributed (in fact they follow an approximate Rayleigh distribution). There are therefore two sets of gaussian-distributed correlation values: one with a mean value of two and a standard deviation of $\sqrt{2A}$ (the "background" correlation values); the other with a mean of unity and the same standard deviation (the "signal" correlation values).

A suitable threshold value is now chosen, such that only rarely is a background correlation value obtained which falls below this threshold, giving rise to a false

match. Setting the threshold at 2.5σ below the background value has been found to be convenient in practice. Once the threshold has been fixed in this way, one may readily deduce how often a "true" match will be detected (ie. a value from the signal distribution which falls below the threshold).

The main error is that the distribution of intensity values in the template is not gaussian. However, a correction factor may be applied which *does* produce an approximately gaussian distribution in the template. Inspection of the distribution of values shows that a majority (70%) of the pixel values in the template lie very close to the mean, giving rise to a spike in the distribution. Removing these pixels from the correlation, results in a probability of detecting a pit which varies with the pit diameter (as shown in fig. 4).

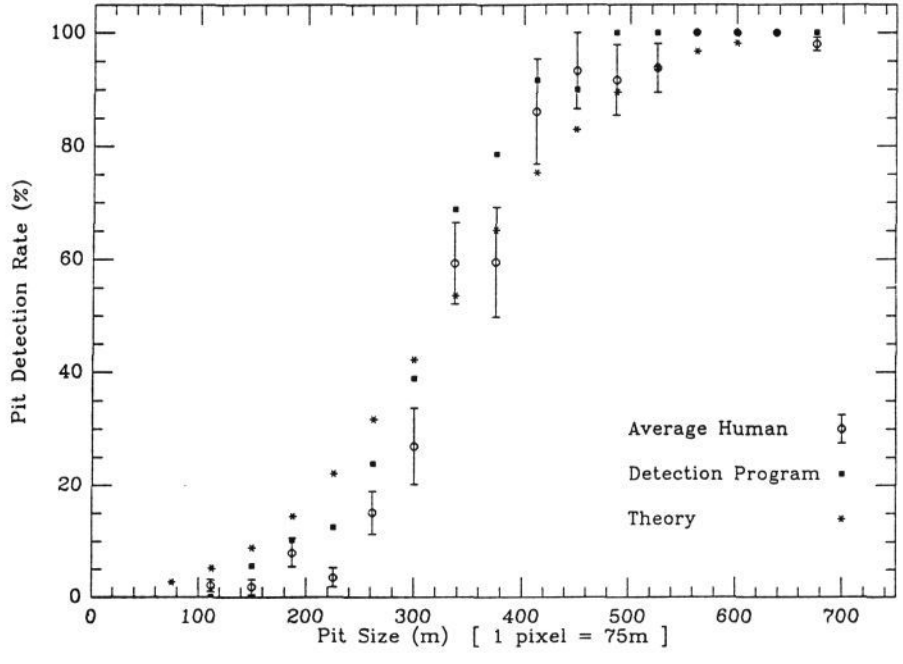

Fig. 4 Comparison of detection rates for simulated pits: humans, machine and theory.

6 Analysis of results

In this section the results of two distinct sets of experiments are presented. First, the outcome of the control experiment involving both human and machine measurements of artificial images is analysed. Second, the results of running the correlation algorithm on Magellan data are assessed, by comparing them with human measurements of the same data.

6.1 Synthetic data

A variety of tests were carried out with different distributions of simulated pit sizes and speckle noise levels. Software routines were developed which logged the (x,y) coordinates where human observers believed that they had detected a pit. Since the

coordinates of the pits were already known, it was possible to calculate the detection rate (and false alarm rate) as a function of pit size. Modified versions of these routines were used to calculate the same quantities for the pit-detection algorithm.

Fig. 4 summarises the results of some of these tests. It shows how the probability of detecting a pit image varies with the pit diameter. Three sets of points are shown: one set is the average for all observers and all pit size distributions; one set is the equivalent for the detection algorithm; and the third set is derived from the theoretical prediction outlined in section 5.

It can be seen that the three sets of data are very similar to each other (the differences between the human results and the machine results are almost within the error bounds for each data point). The departure of the theoretical curve from the machine results is readily explained, as being due to the approximations used in deriving the theory. What is perhaps of more interest, is the similarity between the machine results and the human results, which suggests that some underlying similarity may exist between two apparently disparate detection mechanisms. In addition, results such as those shown in fig. 4 can be used to provide corrections to pit size-distributions derived previously by human observers (eg. [3]).

6.2 Magellan data

To date, the algorithm has only been run with a very limited number of Magellan images for which human observations are available (eg. fig. 1). The results of this comparison between the pit detection rates of humans and the machine, using real Magellan images, are shown in table 1.

Table 1 Pit Detection Results for Real Data

MGN Image	Observer	No. seen by observer	Seen by observer only	Seen by machine & observer	Seen by machine only	No. seen by machine
1	CRW	42	4	38	3	41
	MRBF	48	10	38	3	41
2	CRW	19	8	11	4	15
	MRBF	37	26	11	4	15
	JEG	18	9	9	6	15
3	CRW	26	7	19	6	25
	MRBF	36	19	17	8	25
	JEG	41	22	19	6	25

From this table it is apparent that there are significant variations in the observations made by humans. It can also be seen that, under certain circumstances, the machine results are very promising: the algorithm performs well on images where the background is relatively uniform (although it has yet to be modified to take account of variations in the background texture which require a variable threshold). Finally, it was also noted that, whilst some of the pits seen by the machine alone were false positives, many represented real features that the humans had missed.

7 Discussion

In this paper, we have described the preliminary results of an investigation into the automatic detection of volcanic features in noisy, radar images. Whilst some progress has been made towards accomplishing this task, we have had to limit ourselves to

detecting the small pits which many, but not all of the volcanoes possess. We have also encountered difficulties when using our algorithm in regions where the background texture is non-uniform.

In the immediate future, we aim to increase the reliability of the algorithm at detecting the pits. It is then intended that as much Magellan data as possible is processed using the improved technique. At the same time, modifications will be made to enable detection of the volcanoes themselves, probably using reduced-resolution Magellan data.

This leads to the question of processing times. At present, running on a Sun SPARCstation 1+, the algorithm is able to scan one 512x512 pixel image, making several passes with different-sized templates, in approximately 30 minutes. For regions with high volcano-densities, this time is comparable to that required by a trained geologist to undertake the same task of recognising and recording the coordinates of all the volcanic edifices. The machine, however, has certain advantages over the human observer. In particular, it could, in principle, process data 24 hours per day with little human intervention. Furthermore, from the experiments conducted with artificial data, it has been discovered that humans occasionally miss large features for which the machine has a consistent, 100% success rate.

In conclusion, therefore, whilst still at a relatively early stage of development, the methods described here appear to have great potential in the fields of planetary science and remote sensing. Data sets in these areas are already reaching sizes that make comprehensive analysis by trained observers impossible. As the processing speeds of relatively inexpensive computers continue to increase, however, automated image-data analysis and reduction will become an increasingly important and effective scientific tool.

Acknowledgements

C.R. Wiles has been supported by a NERC Ph.D. studentship during the course of this research.

We acknowledge the Magellan project at the NASA Jet Propulsion Laboratory, for the provision of radar image data of Venus.

References

[1] JPL D-6724, Magellan science requirements document, **630-6 (Rev. D)**. California Institute of Technology, Pasadena, 1991, pg 2-1.

[2] G.H. Pettengill, P.G. Ford, W.T.K. Johnson, R.K. Raney and L.A. Soderblom, Magellan: radar performance and data products. *Science* 1991; **252**: 260-265.

[3] J.C. Aubele and E.N. Slyuta, Small domes on Venus: characteristics and origin. *Earth, Moon and Planets* 1990; **50/51**: 493-532.

[4] J.E. Guest, M.H. Bulmer, J.C. Aubele, et al., Small volcanic edifices and volcanism in the plains of Venus. *J. Geophys. Res.* 1992; (in press).

[5] R.S. Saunders, G.H. Pettengill, R.E. Arvidson, et al., The Magellan Venus radar mapping mission. *J. Geophys. Res.* 1990; **95**: 8339-8355.

[6] J.P. Secilla, N. Garcia and J.L. Carrascosa, Template location in noisy pictures. *Signal Processing* 1988; **14**: 347-361.

[7] J. Thomas, Radar image simulation. In: Leberl F.W. Radargrammetric image processing. Artech House, Boston London, 1990, pp 165-187.